Microphysical and radiative evolution of aerosol plumes over the tropical North Atlantic Ocean

Timothy J. Garrett,[1,2] Lynn M. Russell,[1,3] V. Ramaswamy,[1,4] Steven F. Maria,[3] and Barry J. Huebert[5]

Received 22 February 2002; revised 29 July 2002; accepted 5 August 2002; published 15 January 2003.

[1] Over the tropical North Atlantic Ocean in the summer, plumes of aerosol extend from Saharan Africa to the Caribbean. The microphysical and radiative evolution of such plumes is studied using a Lagrangian column model and measurements obtained near the west coast of Africa (during the second Aerosol Characterization Experiment [ACE-2]) and the Caribbean Sea (during the Passing Efficiency of the Low Turbulence Inlet [PELTI] experiment). Mass and scattering in the plumes can be separated into two layers that overlay one another over much of the Atlantic Ocean. Mineral dust dominates in the lower free troposphere, and sea-salt aerosol dominates in the boundary layer. Carbonaceous, sulfate, and nitrate (CSN) aerosols are a minor component of mass but contribute significantly to total column optical depth. Combined, CSN aerosols and sea-salt contribute to more than half of total aerosol clear-sky shortwave forcing associated with such plumes. Satellite and model data suggest that the reduction of plume forcing between the African coastline and the Caribbean is less than ~20%. The reduction is due principally to settling of large dust particles and atmospheric subsidence; however, the reduction of forcing remains small because (a) boundary layer trade winds provide a steady source of sea-salt, (b) dust particles are initially elevated 2.5–5.5 km from the surface and therefore have long settling distances before removal, and (c) small CSN and dust particles in the free troposphere have high specific extinction and lack significant removal processes. Measurements and climatology suggest that the CSN aerosols in the free troposphere are anthropogenic pollution from Europe. *INDEX TERMS:* 0305 Atmospheric Composition and Structure: Aerosols and particles (0345, 4801); 3337 Meteorology and Atmospheric Dynamics: Numerical modeling and data assimilation; 3359 Meteorology and Atmospheric Dynamics: Radiative processes

Citation: Garrett, T. J., L. M. Russell, V. Ramaswamy, S. F. Maria, and B. J. Huebert, Microphysical and radiative evolution of aerosol plumes over the tropical North Atlantic Ocean, *J. Geophys. Res.*, *108*(D1), 4022, doi:10.1029/2002JD002228, 2003.

1. Introduction

[2] There are three principal categories of aerosols that contribute to clear-sky aerosol climate forcing over the oceans: Wind-generated mineral dust, wind-generated sea-salt particles, and carbonaceous, sulfate, and nitrate (hereafter CSN) aerosols from biogenic and anthropogenic sources. *Haywood et al.* [1999] estimated globally averaged clear-sky aerosol forcing over oceans ranges from -1.5 to -5.0 W m^{-2} for sea-salt, compared with -2.5 W m^{-2} for anthropogenic sulfate, natural sulfate and carbonaceous aerosol combined, and -1.1 W m^{-2} for mineral dust. Regionally, however, the highest values of ocean aerosol optical depth (with the exception of the Indian Ocean in the summer) are associated with a broad plume of aerosol that extends downwind of the West African coast [*Prospero*, 2002]. NIMBUS-7 Total Ozone Mapping Spectrometer (TOMS) aerosol absorption index (AI) data show that this plume is associated with mineral aerosol. The magnitude of the clear-sky aerosol direct radiative forcing in this plume, averaged between January and September, is as high as ~ -20 W m^{-2} close to the African coast [*Loeb and Kato*, 2002].

[3] Transport of mineral aerosol over the Atlantic Ocean follows a seasonal pattern (Prospero, submitted manuscript, 2001). In the summer, surface air masses are transported southward over the Mediterranean Sea to the Saharan Desert. Desert soil has a low heat capacity and surface air temperatures over the Sahara reach up to 70°C. The heating creates a mixed-layer, sometimes in excess of 4 km deep, filled with fine eolian dust [*Dubief*, 1977]. The dust layer surmounts cooler maritime boundary layer or monsoonal air to the west and south, and forms a hot dust-filled layer in

[1]Atmospheric and Oceanic Sciences Program, Princeton University, Princeton, New Jersey, USA.
[2]Now at Meteorology Department, University of Utah, Salt Lake City, Utah, USA.
[3]Department of Chemical Engineering, Princeton University, Princeton, New Jersey, USA.
[4]Geophysical Fluid Dynamics Laboratory, NOAA, Princeton, New Jersey, USA.
[5]School of Ocean and Earth Science and Technology, University of Hawaii at Manoa, Honolulu, Hawaii, USA.

0148-0227/03/2002JD002228$09.00

Table 1. Summary of Measurements Obtained During ACE-2 and PELTI

	ACE-2 Measurements	PELTI Measurements
Location	West African coast (27°N, 16°W)	Caribbean (12° to 19° N, 59° to 63°W)
Dates	8 July, 17 July 1997	9 July, 15 July, 19 July, 21 July 2000
Measurements	Flight profiles to 3700 m [*Collins et al.*, 2000] Ground based at 2360 m [*Formenti et al.*, 2000]	Horizontal flight legs in MBL and FT, profile to 5700 m on 21 July
Size distributions	Airborne DMA and PCASP-100X (D < 4 μm) Ground based almuncantar (D < 20 μm)	Airborne DMA, PCASP-100X and FSSP-300 (D < ~20 μm)
Chemical composition	Ground-based and size-resolved in MBL and FT	Airborne submicron and bulk
Meteorological profiles	Balloon	Airborne
References	*Collins et al.* [2000]; *Formenti et al.* [2000]	*Maria et al.* [2002]; Huebert et al. (submitted manuscript, 2002)

the lower free troposphere ~3 km deep. This air mass is termed the Saharan Air Layer (SAL). The large temperature gradient between the Sahara and cooler equatorial air generates an easterly wave disturbance [*Reed et al.*, 1977] centered near 650 mb at 17°N that transports the dust to the Caribbean in between 5 and 7 days [*Prospero and Carlson*, 1972]. In situ measurements show the volume size distribution of SAL aerosol has a pronounced mode between 4 and 10 μ m diameter [*Prospero and Carlson*, 1972; *Carlson and Caverly*, 1977; *Talbot et al.*, 1986; *Formenti et al.*, 2000].

[4] It is often assumed that, since a region of high optical depth extends west of the Saharan desert, and that large quantities of dust are carried downwind of the African continent, dust is the dominant component of summertime optical depth and clear-sky radiative forcing over the tropical North Atlantic Ocean [e.g., *Schulz et al.*, 1998; *Cakmur et al.*, 2001] (see also *Prospero* [2002]). Other measurements suggest sea-salt and CSN aerosol are a component of aerosol optical depth over the Atlantic Ocean downwind of the Saharan Desert. For example, atmospheric profiles presented by *Collins et al.* [2000] suggest that surface aerosol extinction, where sea-salt dominates, is comparable to aerosol extinction in the free-troposphere, where dust dominates. *Kahn et al.* [2001], using recent Multiangle Imaging Spectroradiometer (MISR) satellite data, showed that between 33% and 46% of July total optical depth, downwind of the West African coast, could be attributed to carbonaceous and sulfate aerosols. Sulfate and carbonaceous aerosols comprised an average 17% of total optical depth measured from the boundary layer at Sal Island, Cape Verde [*Chiapello et al.*, 1999] and 44% of optical extinction, annually averaged, measured in the lower free-troposphere at Tenerife, Canary Islands [*Maring et al.*, 2000]. Additionally, S. Kinne et al. (Monthly averages of aerosol properties: A global comparison among models, satellite data and AERONET ground data, submitted to *Journal of Geophysical Research*, 2001), has noted that general circulation models show particularly pronounced disagreement when describing the contributions of different aerosol types to the aerosol optical depth field downwind of the Saharan desert.

[5] The goal of this paper is to evaluate a) the microphysical and clear-sky radiative evolution of the SAL and b) the relative importance of various aerosol types in the MBL and SAL to clear-sky optical depth and direct shortwave radiative forcing over the tropical North Atlantic Ocean. The study focuses on the month of July, when dust is transported to the Caribbean. We use measurements of dust events previously obtained off the West African coast during the second Aerosol Characterization Experiment (ACE-2), and new measurements from the Caribbean obtained during the Passing Efficiency of the Low Turbulence Inlet (PELTI) experiment. The types of measurements obtained during ACE-2 and PELTI are summarized in Table 1. ACE-2 and PELTI provided a detailed characterization of the chemistry and microphysics of aerosols over the North Atlantic Ocean. In particular, two days during ACE-2 provided detailed measurements during dust events. These two cases are used to initialize an externally and internally mixed, size-and-composition-resolved 1-D column aerosol microphysical model that is linked with an accurate broadband shortwave radiative transfer code (section 2.1). Explicit generation of dust, continental, and oceanic aerosol in the model is not considered in the model. Rather, the focus is on aerosol microphysics and clear-sky radiative forcing over the ocean. The model is allowed to evolve along an assumed trajectory, from Africa across the tropical North Atlantic Ocean (Figure 1), to yield projected microphysical and radiative properties of the aerosol plume in the Caribbean (section 2.3). The model results are then com-

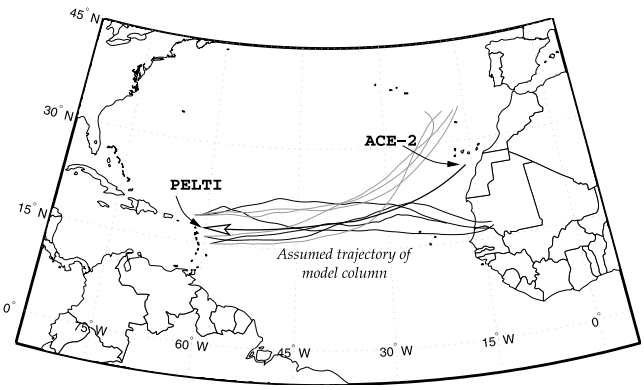

Figure 1. Approximate locations of measurements obtained during dust events during the July 1997 ACE-2 and July 2000 PELTI field projects, and assumed trajectory of the Lagrangian column model used in this study (black arrow). Thin lines are 7-day HYSPLIT4 isobaric air mass back-trajectories (obtained from http://www.arl.noaa.gov/ready/hysplit4.html) from measurement points during PELTI at altitudes representative of the marine boundary layer (gray, ~500 m altitude) and the Saharan air layer (black, ~2500 m altitude).

pared with measurements obtained in PELTI (section 2.3). The implication of the measurements and results to the radiative evolution over the Atlantic Ocean is discussed in section 4.

2. Modeled Evolution of Aerosol Plumes Over the Tropical North Atlantic Ocean in July

2.1. Model Description

[6] This study explores the microphysical and radiative evolution of aerosol plumes over the tropical North Atlantic Ocean using a one-dimensional Lagrangian column model. The advantage of a column model is that computational expense can be devoted to explicit microphysical calculations.

2.1.1. Microphysical Model

[7] Modeled optical properties and radiative forcing by plumes containing mineral aerosol are highly sensitive to prescribed size distributions and composition of mineral aerosol [*Tegen and Lacis*, 1996; *Claquin et al.*, 1998; *Sokolik and Toon*, 1999]. It is, therefore, important to explicitly describe the size-resolved internal and external composition of the size distribution. The microphysical and chemical component of the model used here is based on a size- and composition-resolved externally mixed aerosol model developed by *Russell and Seinfeld* [1998]. Both mass and number of externally and internally mixed aerosol size distributions are explicitly resolved. The model is discretized into a column of vertically fixed layers, 750 m thick from the surface to 1500 m altitude (which is the nominal top of the MBL), and 500 m thick from the top of the MBL to the top of the SAL. Within each layer, aerosol size distributions are binned into 35 sizes, initially ranging logarithmically from 0.01 to 30 μm diameter. The total particle size distribution is divided into six externally mixed size distributions, each representing an aerosol "type". The aerosol types are considered: "calcite-dominant", "quartz-dominant", "clay-dominant", "sulfate-dominant", "soot-dominant", and "sea-salt-dominant". Within each particle type, particles in each size bin are composed of an explicitly defined internal mixture of chemical "species". We consider eight aerosol chemical species in our model: water, sodium chloride, ammonium sulfate, black carbon, quartz, clay aggregates, calcite, and gypsum. Nitrate and organic aerosol species are also a significant component of aerosol, however we treat them as sulfate aerosol due to their similar optical properties at visible wavelengths (although water uptake at high relative humidity will differ). Particle number, size and composition evolve due to heterogeneous chemical reactions with gas phase species, condensation, coagulation, and vertical removal from dry deposition, wet deposition, entrainment, atmospheric subsidence or lifting. Preceding rate calculations, the equilibrium water content of a particle in subsaturated conditions (defined such that the surface and ambient vapor pressures are equivalent) is calculated based on the humidity, temperature, solute activity, size and number concentration of particles (relative humidity vertical profiles are held constant). The solute activity is determined from concentrations of Cl^-, OH^-, $SO_4^=$, Na^+, H^+, and NH_4^+ using the Pitzer method [*Zemaitis*, 1986]. Mineral components of aerosol are assumed to be nonhygroscopic [*Li-Jones et al.*, 1998], although coatings of condensed electrolytes may take up water.

[8] This study uses a Lagrangian "moving-section" scheme [cf. *Warren and Seinfeld*, 1985] to track particle size as it grows due to coagulation and condensation of trace gas species. The coagulation algorithm used in this study conserves both mass and number while tracking the redistribution of chemical species between different particle types. The type assignment of a particle newly formed by coagulation is allocated to the type assignment of the largest of the constituent coagulating particles. For example, the coagulation of a 5.0 μm "clay-dominant" *type* particle with a 0.1 μm "sulfate-dominant" *type* particle creates a new "clay-dominant" *type* particle composed mostly of an internal mixture of clay mineral *species* with a new added component of ammonium sulfate *species*. The coagulation kernel includes coagulation due to Brownian motion and gravitational settling.

[9] Model layers are assumed to be fixed and horizontal divergence is ignored. Therefore, the continuity equation for aerosol mass and number transfer between layers includes gravitational settling, entrainment, and atmospheric subsidence/lifting. Precipitation removes particles directly from the column according to a specified timescale. Beneath the warm, thermodynamically stable SAL, precipitation is limited to the boundary layer [*Prospero and Carlson*, 1972; *Talbot et al.*, 1986], where the lifetime of aerosol over the ocean is assumed to be 3 days [*Twomey and Wojciechowski*, 1969]. Even though dust particles have low hygroscopicity, they are observed in raindrops [*Gonzales and Murr*, 1977], and are therefore included among precipitable species. MBL sea-salt aerosol are assumed to be in steady state. Vertical diffusion is ignored as the SAL is thermodynamically stratified and laminar.

[10] The model permits new sulfate formation in three ways. First, SO_2 in the atmosphere may be oxidized by the OH radical to form H_2SO_4 molecules that may condense directly onto particles. Second, SO_2 condenses directly onto particles where, in the presence of water, it is oxidized by dissolved H_2O_2 and O_3. Third, SO_2 that condenses on calcite particles ($CaCO_3$) is subsequently converted to gypsum $CaSO_4 \cdot 2H_2O$ by way of calcium sulfite hemihydrate ($CaSO_3 \cdot \frac{1}{2}H_2O$) [*Dentener et al.*, 1996; *Böke et al.*, 1999]. *Herring et al.* [1996] measured a quasi-second order reaction rate of SO_2 with dust over Kuwait. The estimated loss rate for SO_2 was $9 \pm 4 \times 10^{-8}$ $(\mu g\ m^{-3})^{-1}\ s^{-1}$. Combining this reaction rate with observed dust size distributions we inferred a value for the uptake coefficient (γ) of SO_2 on calcite of 1.2×10^{-3}. This value is in good agreement with laboratory measurements that suggest an upper limit for γ of 4×10^{-3} [*Ullerstam et al.*, 2001]. Although included, none of the above three processes played a significant role in the model calculations presented in this study.

[11] The 1-D microphysical model described here has several limitations: it requires accurate initialization, it assumes zero vertical wind shear, and that column layers are horizontally homogeneous, or that divergence of the horizontal wind field is negligible. However, isobaric air mass back-trajectories from PELTI (Figure 1) indicate that, although air masses in the MBL and SAL had different origins, their trajectories showed little daily variability and

they were collocated at ~20°N over most of the Atlantic Ocean. Further, *Carlson and Prospero* [1972] showed that dust concentrations in the boundary layer are determined principally by vertical mixing between the MBL and the SAL, and that the SAL can be thought of as a "somewhat leaky duct".

[12] A limitation of this study is it ignores several processes that affect aerosol size distributions in the MBL, such as nucleation, cloud processing, and dynamic boundary layer thickness [*Johnson et al.*, 2000]. However, nucleation does not significantly affect concentrations of particles responsible for radiative forcing, MBL cloudiness is suppressed in the wake of dust plumes [*Carlson and Prospero*, 1972], and this study is limited to studying plume evolution on weekly rather than the diurnal timescales that affect MBL thickness.

2.1.2. Radiative Transfer Model

[13] The shortwave time-dependent single-scattering properties of an aerosol depend on the shapes, sizes and refractive indices of its constituent particles. The complex refractive indices for soot [*Querry*, 1987], calcite, quartz, gypsum and ammonium sulfate [*Ivlev and Popova*, 1972], clays [*Patterson*, 1977; *Patterson et al.*, 1981; *Querry*, 1987], sea-salt [*Shettle and Fenn*, 1979] and water [*Segelstein*, 1981] are discretized into 42 wavelengths quasi-logarithmically spaced between 0.2 and 6.0 μm. The refractive indices of internally mixed aerosol composed of more than two species are calculated from the volume-averaged mean complex dielectric constant, in which case $\bar{N} = \sqrt{\bar{\epsilon}}$. Volume-averaging yields identical results to several other commonly used approaches (such as the effective-medium or Maxwell-Garnett approximation) provided the components of the particle are dielectrically similar [*Bohren*, 1986].

[14] The time-dependent optical depth (τ), single-scattering albedo (ω_0), and asymmetry parameter (g) of each model layer are calculated for each particle type assuming the particles are spheres. Aerosol particles are frequently irregular shapes, particularly in dust layers. Differences between the phase function for spherical and irregularly shaped dust particles can be large [*Mishchenko et al.*, 1997]. However, this study is concerned with flux rather than radiance calculations, in which case g is a sufficient representation of the angular distribution of scattering. Using a theoretical model for representing light scattering by irregularly shaped dust particles, Mishchenko et al. found that errors in τ, ω_0, and g associated with neglecting particle asphericity are never more than 2% for size distributions representative of those described in this study.

[15] We calculate clear-sky top-of-the-atmosphere shortwave radiative fluxes and solar heating profiles using a solar radiative transfer model [*Freidenreich and Ramaswamy*, 1999]. The model includes particulate scattering and absorption, Rayleigh scattering, and gaseous absorption by O_2, O_3, CO_2, and H_2O. The solar spectrum is divided into 25 pseudo-monochromatic bands between 0 and 57,600 cm^{-1}. Aerosol single-scattering properties are integrated into the 25 band radiative transfer model using a solar-flux weighted averaging scheme. Reflection and transmission for homogeneous layers is calculated using the δ-Eddington method. An "adding" technique is used to solve for vertical fluxes and heating rates. Compared to reference calculations without cloud or aerosol, the calculations of heating rates are accurate to within 10%, and within 2% for atmospheric absorbed flux.

[16] The direct, diurnally averaged top-of-the-atmosphere clear-sky direct radiative forcing (TOAF) by an aerosol type, or all aerosol particles combined, is assumed to be:

$$\mathrm{TOAF}_{particles} = \left[\mathrm{TOAF}_{gases}(\bar{\mu}_0) - \mathrm{TOAF}_{particles+gases}(\bar{\mu}_0)\right] \times (\text{day length/solar period}) \quad (1)$$

where, the forcing-weighted mean solar zenith angle, $\bar{\mu}_0$, is chosen such that $\mathrm{TOAF}_{gases}(\bar{\mu}_0) = 2\int_0^1 \mu_0 \mathrm{TOAF}_{gases}(\mu_0)$. Solar calculations in the model are made for 15 July at 17°N. Note that TOAF is a negative quantity. $\mathrm{TOAF}_{gases}(\mu_0)$ depends on the representation of ocean surface albedo, $R_s(\mu_0)$, which is defined here by *Taylor et al.* [1996]:

$$R_s(\mu_0) = \frac{0.037}{1.1\mu_0^{1.4} + 0.15} \quad (2)$$

2.2. Model Initialization

[17] To study the evolution of aerosol plumes across the tropical North Atlantic we initialize this model using data from the east side of the tropical North Atlantic Ocean obtained during ACE-2. ACE-2 was based out of Tenerife, Canary Islands during June and July 1997.

[18] Data from ACE-2 used in this paper are described by *Collins et al.* [2000], *Formenti et al.* [2000], *Putaud et al.* [2000], and *de Reus et al.* [2000], and are available through the ACE-2 database (http://ultra.ei.jrc.it:8181/). We limit this study to two cases on 8 July and 17 July 1997 when vertically resolved airborne, ground-based and balloon measurements were obtained for a free-troposphere containing a mineral dust haze layer. Meteorological profiles were obtained from sounding data shown in Figure 2. Dried aerosol size distributions described by *Collins et al.* [2000] and available from the ACE-2 archive were binned and averaged according to model layer altitude. Where data for large aerosol were unavailable, composite aerosol spectra were derived from ground-based measurements of the same dust events obtained by *Formenti et al.* [2000] (section 3.2.2). Where aircraft measurements described by *Collins et al.* [2000] did not extend to the top of the SAL, aerosol concentrations were extrapolated assuming concentration was proportional to pressure [*de Reus et al.*, 2000].

[19] Thermodynamic profiles (provided by the Meteorological Service of Santa Cruz de Tenerife, Canary Islands, and obtained from the ACE-2 database), concentrations of particles larger than 0.12 μm [*de Reus et al.*, 2000; *Collins et al.*, 2000], and wind profiles measured on 8 July and 17 July 1997 are shown in Figure 2. The SAL was a ~3 km thick layer, with elevated values of relative humidity and particle concentrations, high temperatures, and low wind shear, capped by a temperature inversion at ~5 km. The temperature profile through the depth of the layer was approximately adiabatic; the potential temperature (θ) was 44.5 ± 0.1° on 8 July, and on 17 July the value of θ was 41° at the bottom and 45° at the top of the SAL. Similar values of θ in the SAL have been reported by *Carlson and Prospero* [1972]. Although the SAL was conditionally unstable, wind shear was very low (wind speeds were 15

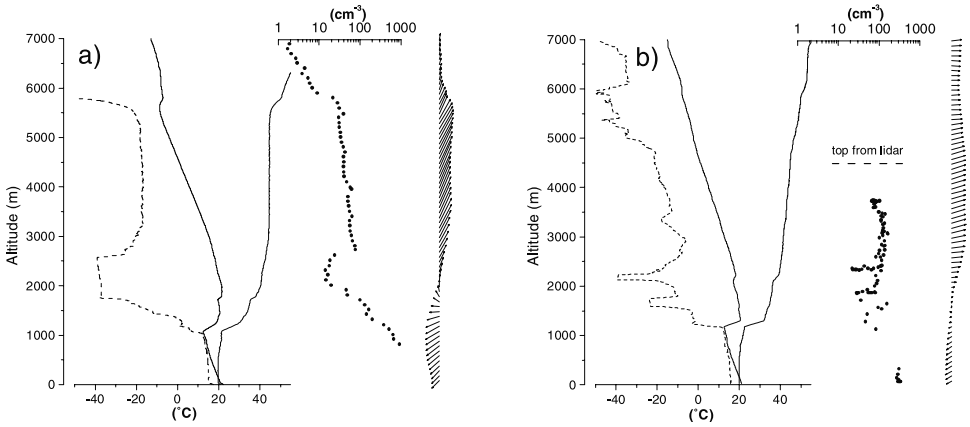

Figure 2. Soundings and measurements of the vertical distribution of particle concentrations of a Saharan air layer topping a marine boundary layer on 8 July (a) and 17 July (b) 1997. Temperature (thin solid), dewpoint (dashed), potential temperature (thick solid) and horizontal wind data (arrows) are obtained from balloon measurements from Tenerife, Canary Islands at 600 UTC on 8 July and 1200 UTC on 17 July. Concentrations of particles (dotted) >0.12 μm diameter were obtained using a PCASP-100X [*Collins et al.*, 2000; *de Reus et al.*, 2000]. The approximate height of the dust layer on 17 July was estimated from lidar measurements [*Welton et al.*, 2000].

± 0.5 m s^{-1} on 8 July and 15 ± 1 m s^{-1} on 17 July) and values of the Richardson number [*Seinfeld and Pandis*, 1998] were 0.6 on 8 July and 50 on 17 July. Inspection of isentropic back trajectories (available at http://www.arl.noaa.gov/ready/sec/traj.html), and Total Ozone Mapping Spectrometer (TOMS) imagery for the days leading up to 8 July and 17 July, suggests that the SAL was near the surface over Mali, Saharan Africa, approximately four to five days prior for each case. The boundary layer air, by comparison, was moist and the potential temperature ∼20° cooler than in the SAL. The boundary layer air had passed over the Iberian peninsula prior to 8 July and the coastal European North Atlantic Ocean prior to 17 July [*Collins et al.*, 2000].

[20] Due the relatively high stability of the SAL, and its warmth relative to the MBL, vertical diffusion and entrainment between the MBL and free troposphere are neglected in the model base case. It is further assumed there is no subsidence in the free-troposphere; the model sensitivity to this assumption is explored in section 2.4.4.

[21] Size distributions of aerosols in the MBL and SAL on 8 July and 17 July are described by *Collins et al.* [2000]. They were obtained from the ACE-2 database, averaged, and binned according to model layer. Concentrations of particles larger than 4 μm in the SAL were inferred from ground-based almuncantar (spectral aerosol optical depth) measurements, obtained at an altitude of 3570 m on 8 July and 17 July [*Formenti et al.*, 2000]. Solutions to a mathematical inversion of spectral optical depth are nonunique, and are sensitive to various assumptions about the optical properties of the aerosol. However, the shape of the size distributions described by Formenti et al. were consistent with in situ ground-based aerodynamic particle sizer (APS) measurements obtained at 2360 m altitude in the Canary Islands in July 1995 during dust events [*Maring et al.*, 2000].

[22] The size-resolved composition of MBL and SAL dry aerosol used to initialize the model is described by *Collins et al.* [2000]. To reduce computational time, while retaining the essential physics necessary to evaluate the microphysical and radiative evolution of the SAL, all sulfate and organic aerosol described by Collins et al. are represented here by the "sulfate-dominant" type aerosol in the model. It is assumed that, initially, all aerosol types are pure external mixtures, except for soot, of which half is assumed to be internally mixed with "sulfate-dominant" type aerosol.

[23] To represent size-dependent absorption by dust aerosol [*Patterson*, 1981], we have used a simplified mineralogy of "calcite-dominant", "clay-dominant" and "quartz-dominant" particles. The exact mineralogical composition of dust aerosol in the Canary Islands was not determined during ACE-2. We therefore estimate dust composition over the tropical North Atlantic Ocean using previously published measurements, and submicron elemental analysis data obtained during PELTI (section 3.3). For the purposes of this modeling study we separate the dust into three particle diameter size ranges: smaller than 1.0 μm, 1.0 to 8.0 μm diameter, and larger than 8.0 μm. Submicron mineralogical ratios were derived from Si/Al and Ca/Al ratios measured during PELTI assuming a) quartz and calcite were pure SiO_2 and $CaCO_3$, respectively, and b) a clay mineral composition (of illite, kaolinite and chlorite) for Caribbean summertime dust [*Glaccum and Prospero*, 1980]. Mineral apportionment in the intermediate size range was inferred from dust composition obtained in Barbados [*Glaccum and Prospero*, 1980] (feldspar, plagioclase and microcline were categorized as quartz). The mineralogy of the largest size range was inferred from surface dust deposits analyzed by *Game* [1962] (feldspar, amphibole, and biotite were categorized as quartz; organic material associated with the dust was neglected). The assumed apportionment of dust minerals within each size range is shown in Table 2.

2.3. Model Evolution

[24] The model microphysics, initialized with data from ACE-2, is allowed to evolve for 7 days in the approximate

Table 2. Apportionment of Saharan Dust Mineral Species in the Initialization of the Base Case Model Runs[a]

	<1 μm	1–8 μm	>8 μm
clays	0.56	0.75	0.41
quartz	0.35	0.20	0.33
calcite	0.09	0.05	0.25

[a]Based on XRF measurements during PELTI and dust mineral data from *Glaccum and Prospero* [1980] and *Game* [1962].

travel time for Saharan aerosol to reach the Caribbean from Africa [*Prospero and Carlson*, 1972]. For simplicity we group aerosol into three categories: "dust" (composed of calcite-dominant, quartz-dominant and clay-dominant "type" aerosol), "sea-salt" (composed of sea-salt-dominant "type" aerosol), and "carbonaceous, sulfate and nitrate (CSN) aerosol" (composed of sulfate-dominant and soot-dominant "type" aerosol) (section 2.1).

2.3.1. Mass Profiles

[25] The vertical profiles of mass concentration are shown in Figure 3. Profiles are initialized with size distribution and size-resolved composition data obtained during ACE-2 (section 2.2). Initially, off the coast of West Africa, the SAL and MBL are in two distinct layers, with maxima at ~4 km altitude and at the surface, respectively, with a minimum at 1.75 km altitude. Maximum mass concentrations in the SAL are 120 μg m^{-3} on 8 July, and 220 μg m^{-3} on 17 July. In the MBL, concentrations are 200 μg m^{-3} on 8 July and 120 μg m^{-3} on 17 July. Aerosol in the SAL are ~80% dust. Aerosol in the MBL are ~90% sea-salt. The boundary layer is more polluted on 8 July than on 17 July (since the MBL air mass had previously passed over the Iberian peninsula).

[26] After 7 days model simulation, there are still two distinct layers. However, the locations of peak concentrations of sea-salt and dust in the Caribbean SAL have settled by ~1 km. CSN aerosol are smaller and do not settle as quickly. Predicted peak dust concentrations in the SAL are 50 μg m^{-3} for the 8 July case, and 130 μg m^{-3} for the 17 July case. A fraction of SAL dust settles into the MBL. MBL dust concentrations increase from almost zero to between 10 and 20 μg m^{-3}.

[27] For comparison, similar dust mass profiles and concentration values were obtained in the Caribbean during the summer of 1969 [*Prospero and Carlson*, 1972]: peak concentrations in the SAL were as high as 160 μg m^{-3}; average dust concentrations were 61 μg m^{-3} in the SAL, compared to 22 μg m^{-3} in the MBL, respectively. Long term average aerosol concentrations measured in the MBL at Barbados are 13 μg m^{-3} for dust, compared to 16.5 μg m^{-3} for sea-salt, and 1.4 μg m^{-3} for non-sea-salt sulfate, nitrate and ammonium combined [*Li et al.*, 1996].

2.3.2. Size Distributions

[28] The model is initialized with vertically resolved size distributions. Aerosol size mass and number distributions in the SAL are shown in Figure 4. Initially, the number size distribution shows two modes. A dust mode, which dominates mass, is located at supermicron sizes; a nucleation mode, which dominates number, has peak concentrations at sizes of 0.06 μm and 0.04 μm diameter on 8 July and 17 July 1997, respectively.

[29] After 7 days of model simulation, coagulation has almost entirely removed particles with diameters smaller than 0.1 μm. Second, particles larger than 3 μm settle out of a layer while being replenished from higher altitudes. The sign of the balance depends on location within the depth of the layer. The aerosol size distributions shown in Figure 4 are from 2750 m altitude in the model. For the 8 July case, the SAL extends to 5.2 km. Relative to initial values, particle concentrations between 2 and 7 μm diameter increase, while concentrations of larger particles decrease. For the 17 July case, the SAL extends to 4.2 km and particle concentrations greater than 4 μm diameter decrease with time.

[30] In the MBL, sea-salt aerosol are assumed to be steady state over the ocean. However, a mode associated with small CSN aerosol is depleted by precipitation. A second mode associated with concentrations of large particles increases due to sedimentation of dust from aloft (Figure 5).

2.3.3. Column-Integrated Bulk Microphysical and Radiative Properties

[31] The aerosol single-scattering properties and TOA clear-sky shortwave radiative forcing were calculated following the procedure outlined in section 2.1.2. Values of ACE-2 and Caribbean column-integrated wet aerosol mass, single-scattering properties and TOA clear-sky shortwave radiative forcing are shown in Tables 3 (8 July case) and 4 (17 July case), respectively.

[32] Initially, the total column mass (M), extinction optical depth at 0.55 μm (τ), and broadband top-of-the-atmosphere clear-sky direct aerosol radiative forcing (TOAF) are similar in both cases. M, τ, and TOAF, are 0.52 g m^{-2}, 0.29, and −8.8 W m^{-2}, respectively, on 8 July, and 0.59 g m^{-2},

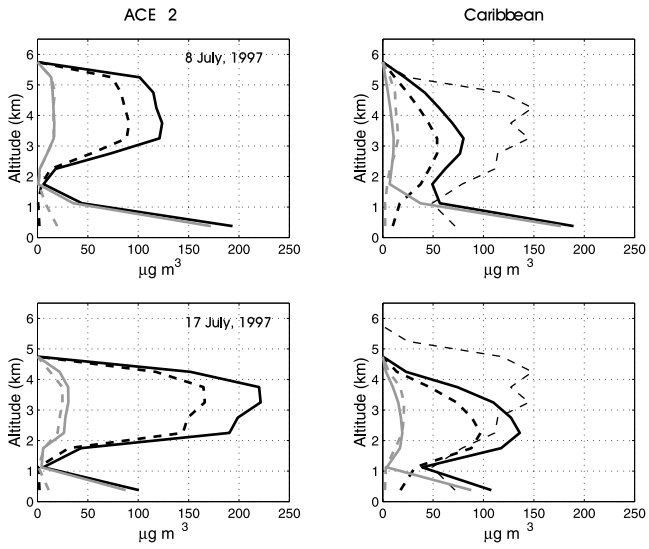

Figure 3. ACE-2 measured profiles of total aerosol mass concentration used to initialize the model [*Collins et al.*, 2000] and predicted profiles in the Caribbean. Solid black, total aerosol; dashed black, total dust; solid gray, sea-salt; dashed gray, chemically generated aerosol ("sulfate-dominant" and "soot-dominant" aerosol types). The thin dashed black line represents concentrations inferred from FSSP-300 measurements obtained on 21 July 2000 during PELTI.

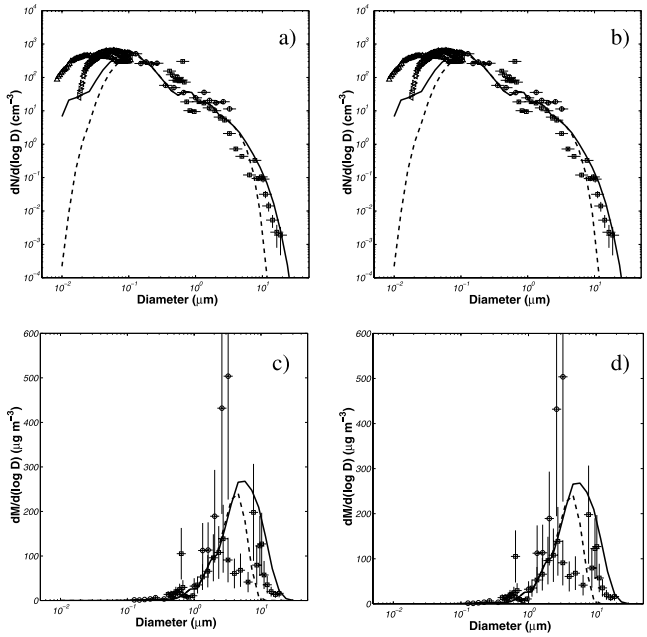

Figure 4. Number and mass size distributions obtained at an altitude of 2750 m during ACE-2 (solid line) on 8 July 1997 (a, c), and 17 July 1997 (b, d) using data obtained by *Collins et al.* [2000] and *Formenti et al.* [2000]. The dashed line represents size distributions predicted by the aerosol model initialized using data from 8 July (a) and 17 July (b). Open symbols represent averaged 1 Hz measurements from PELTI obtained in hazy air at an average altitude of 2750 m during 6 ~1 h horizontal flight legs on 9, 15, 19 and 21 July 2000. Triangles represent data collected using a differential mobility analyzer averaged over ~5 min from 15 July (left pointing), 19 July (right pointing) and 21 July (upward pointing); circles represent data from the PCASP-100X; squares represent data collected using the FSSP-300. Error bars represent instrumental uncertainty. Concentration variability between flight legs was ~30%.

0.29, and −10.1 W m^{-2}, respectively, on 17 July. Dust (0.25 g m^{-2} on 8 July and 0.39 g m^{-2} on 17 July) and sea-salt (0.2 g m^{-2} on 8 July and 0.14 g m^{-2} on 17 July) dominate total column mass. However, CSN aerosol contribute substantially to optical depth. This is because the normalized optical depth (τ/M) for CSN aerosol is, on average, 1.59 m^2 g^{-1} compared to 0.32 m^2 g^{-1} for dust and 0.45 m^2 g^{-1} for sea-salt.

[33] Clear-sky radiative forcing (TOAF) by aerosols is a function of the single-scattering albedo, ω_0, the asymmetry parameter, g, and τ. Low values of ω_0 correspond to higher aerosol absorption and lower TOAF. Low values of g correspond to greater aerosol backscatter and higher TOAF. At 0.55 μm wavelength, dust and CSN aerosol have similar values of ω_0. The higher value of ω_0 for the 8 July case compared to the 17 July case reflects the lower contribution of black carbon to total CSN aerosol on that day [*Collins et al.*, 2000]. Sea-salt is transparent. Values of g are lowest for CSN aerosol and largest for sea-salt; in general large particles (such as sea-salt) preferentially scatter light in the forward direction. Initially, CSN aerosol contribute to ~36% of τ on 8 July and 17 July. For TOAF, however, dust and sea-salt dominate, whereas CSN aerosol contributes to ~20% of total forcing. The difference between the normalized forcing (TOAF/M) of CSN aerosol (~−27 W g^{-1}), and that of dust (~−20 W g^{-1}) and sea-salt (−14 W g^{-1}), is smaller than the corresponding differences associated with the normalized optical depth (τ/M). This may be due to the influence of vertical structure on radiative forcing by absorbing aerosol, and also due to conversion of solar energy to diabatic heating within CSN aerosol layers, which reduces their contribution to reflectivity. In the SAL, diabatic heating is due to embedded soot and dust. Calculated peak diabatic heating rates in the SAL are 0.14 K day^{-1} for the 8 July case and 0.23 K day^{-1} for the 17 July case. In the MBL, diabatic heating is due primarily to near-infrared absorption by water associated with deliquesced sea-salt; peak MBL diabatic heating rates are 0.3 K day^{-1} for the 8 July case and 0.17 K day^{-1} for the 17 July case. *Carlson and Caverly* [1977] calculated similar diabatic heating rates for SAL dust with similar values of τ, however they omitted heating by CSN aerosol and MBL sea-salt.

[34] Following trans-Atlantic transport, total column mass decreases by 20% for the 8 July case and 32% for the 17 July case. The single-scattering parameters, ω_0 and g, stay approximately unchanged during trans-Atlantic transport. The optical depth, however, falls off by about 20% for both cases. The magnitude of total clear-sky TOAF decreases by 12% for the 8 July case and 21% for the 17 July case (note that TOAF is a negative quantity).

[35] Diminution of direct radiative forcing by the plume during transport is due primarily to the high settling speeds of large dust particles and the absence of dust sources over the ocean. Initial altitude of the SAL may also make a difference; dust is removed more rapidly from the column on 17 July than on 8 July when the SAL is higher in the free troposphere.

[36] Modeled values for ω_0 (0.88) for SAL dust are identical to in situ nephelometer and particle soot absorption photometer (PSAP) aircraft measurements obtained in Saharan dust off the West African coast [*Haywood et al.*, 2001]. Modeled values of τ (~0.3) near Africa are consistent with mean summer Advanced Very High Resolution Radiometer (AVHRR) aerosol optical depth retrievals for

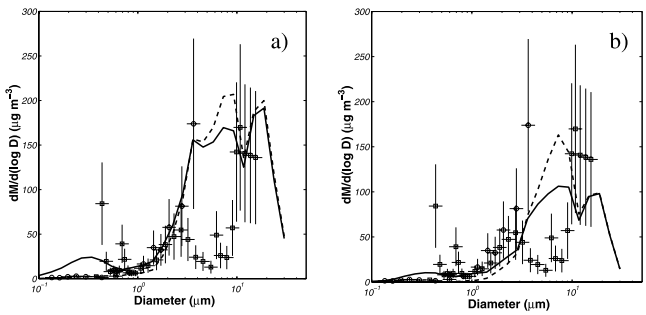

Figure 5. As for Figure 4, except mass distributions are from the lower MBL. Measured values represent an average of 10 h flight time in the lower MBL during PELTI on days when a dust layer was aloft. With the exception of PCASP-100X data (circles), size distributions are representative of ambient RH.

Table 3. Initial Values of Wet Column Mass (M), Clear-Sky Shortwave Aerosol Broadband Radiative Forcing (TOAF), Optical Depth (τ), Single-Scattering Albedo (ω_0), Asymmetry Parameter (g) (at 0.55 μm wavelength), the Ratio of Optical Depth to Column Mass and the Ratio of Aerosol Forcing to Column Mass, and the Change to These Parameters Following 7 Days of Simulated Evolution of Aerosol Size Distributions[a]

	M, g m^{-2} (Δ, %)	τ (Δ, %)	ω_0 (Δ, %)	g (Δ, %)	TOAF, W m^{-2} (Δ, %)	τ/M, m^2 g^{-1} (Δ, %)	TOAF/M, W g^{-1} (Δ, %)
Total	0.52 (−20)	0.29 (−21)	0.94 (−1)	0.75 (2)	−8.8 (12)	0.55 (−1)	−17 (9)
Dust	0.25 (−30)	0.08 (−13)	0.88 (0)	0.77 (−1)	−3.6 (21)	0.31 (23)	−14 (12)
CSN	0.07 (−30)	0.11 (−45)	0.93 (−5)	0.68 (4)	−1.7 (14)	1.63 (−21)	−26 (24)
Seasalt	0.20 (−5)	0.10 (1)	1.00 (0)	0.80 (−1)	−3.6 (5)	0.49 (5)	−18 (−1)

[a]The model is initialized using the size distributions and profiles shown in Figures 3 and 4 from ACE-2 on 8 July 1997. CSN refers to carbonaceous, sulfate, and nitrate aerosol consisting of combined ''sulfate-dominant'' and ''soot-dominant'' type aerosol in the model.

this location [*Cakmur et al.*, 2001] and daily values from a three-dimensional model of a dust plume over the Atlantic Ocean during July [*Schulz et al.*, 1998]. Schulz et al. obtained a ∼40% decrease in τ following transport, which is faster than values obtained here. However, Schulz et al. did not include contributions from CSN aerosols, which are smaller and ∼30% less dense than dust (and therefore settle slower), or sea-salt which has a source over oceans. GCM studies by *Tegen et al.* [1997] show τ is ∼0.14 during the summer over the tropical North Atlantic Ocean, which is below results in this study, but represents an average over periods with and without Saharan aerosol plumes. Nine-month averaged satellite measurements of TOAF show a ∼60% decrease between the East and West sides of the Atlantic [*Loeb and Kato*, 2002]. A possible explanation for the difference between these measurements and our model results is that the nine-month period included the March–April ''Harmattan'' dust period. Harmattan dust particles are transported across the Atlantic Ocean closer to the surface rather than in a SAL [*Dubief*, 1977]. Consequently, they may be more susceptible to rainout and removal by dry deposition.

2.3.4. Column-Integrated Mass and Optical Depth Distributions

[37] Following trans-Atlantic transport, the mode size of the column integrated mass size distribution shifts from a broad peak centered at ∼6 μm diameter to a narrower peak at ∼4.5 μm diameter (Figures 6 and 7). The peak in the aerosol extinction curve shifts from 3.5 μm to 2.5 μm during trans-Atlantic transport. Dry deposition preferentially removes larger particles.

[38] Due to the high specific extinction of submicron CSN aerosol, the column integrated optical depth size distribution curve is significantly broader than the mass size distribution curve. For the 8 July case during ACE-2, submicron aerosol extinction was dominated by boundary layer CSN aerosol. MBL CSN particles are removed by wet deposition. In the Caribbean, the primary contributors to submicron aerosol extinction within the free-troposphere were CSN aerosol for both cases. Due the aridity of the SAL and their small sizes, these aerosol have long lifetimes.

2.4. Sensitivity Studies

[39] The model used to calculate the results described in section 2.3 includes several processes, and the results it yields depend on prescribed initial conditions. In the 17 July base case, clear-sky TOAF decreased by 21% to −8.0 W_m^{-2} during the 7-day simulated plume transport to the Caribbean (Table 4). This section describes the sensitivity of this result to several model processes and initial parameters. We show that model results are sensitive to atmospheric subsidence and assumed mineral composition and insensitive to aerosol coagulation, wet deposition rates, and particle asphericity.

2.4.1. SAL Height

[40] Model results show that the initial height of the layer plays an important role in the radiative evolution of the SAL over the Atlantic Ocean. The dusty SAL measured on 17 July extended between 2.2 and 4.2 km altitude, compared with 2.8 and 5.2 km altitude on 8 July. Since particles from the 17 July case had, in general, a shorter distance to settle, the modeled decrease in TOAF was 21% compared with 12% on 8 July.

2.4.2. Wet Deposition

[41] The progression of a pulse of dust-laden, high potential temperature air across the Atlantic Ocean suppresses boundary layer convective cloudiness and precipitation in its wake [*Carlson and Prospero*, 1972; *Reed et al.*, 1977]. In the base case of the model we assumed the lifetime of aerosol was 3 days. To examine the sensitivity of dust forcing to suppressed precipitation we increased non-sea-salt aerosol boundary layer lifetime by a factor of two, to 6 days. In this case, TOAF in the Caribbean is just 3% higher. This lack of sensitivity is because MBL aerosol (other than sea-salt, which is assumed to be

Table 4. As for Table 2 Except the Model is Initialized Using the Size Distributions and Profiles Shown in Figures 3 and 4 From ACE-2 on 17 July 1997

	M, g m^{-2} (Δ, %)	τ (Δ, %)	ω_0 (Δ, %)	g (Δ, %)	TOAF, W m^{-2} (Δ, %)	τ/M, m^2 g^{-1} (Δ, %)	TOAF/M, W g^{-1} (Δ, %)
Total	0.59 (−32)	0.29 (−19)	0.91 (0)	0.75 (0)	−10.1 (21)	0.48 (19)	−17 (16)
Dust	0.39 (−38)	0.13 (−19)	0.88 (1)	0.77 (−1)	−5.5 (28)	0.33 (31)	−14 (16)
CSN	0.06 (−18)	0.10 (−24)	0.87 (−2)	0.71 (0)	−1.8 (11)	1.54 (−7)	−29 (9)
Seasalt	0.14 (−21)	0.06 (−10)	1.00 (0)	0.79 (0)	−3.0 (19)	0.41 (14)	−22 (2)

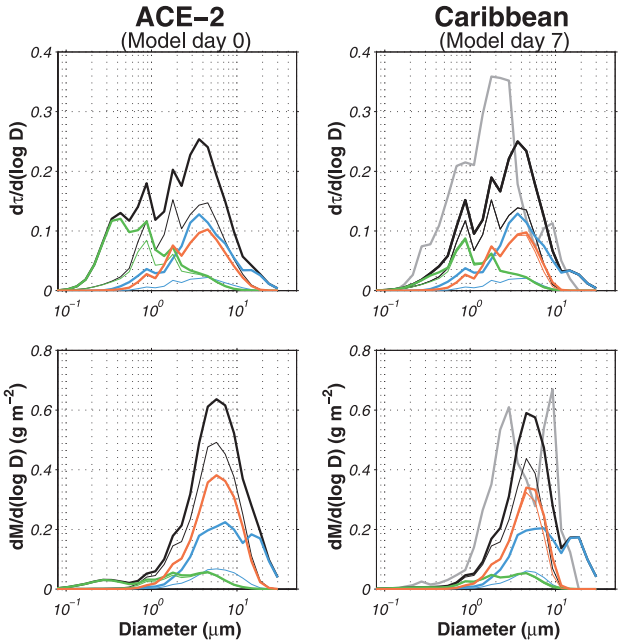

Figure 6. Composition and size resolved aerosol optical depth, at 0.55 μm wavelength, and column mass distributions for the 8 July 1997 initialization from ACE-2, and simulated distributions for the Caribbean. Column-integrated quantities (thick lines) are separated into total aerosol (black), sea-salt aerosol (blue), dust aerosol (red), and CSN aerosol consisting of "sulfate-dominant" and "soot-dominant" aerosol combined (green). Thin lines represent the contribution of aerosol within the free-troposphere (above 1500 m in the model) to the column-integrated total (same color key). The gray line represents total column-integrated optical depth and mass distributions measured during PELTI on 21 July 2000. Note the 8 July integrated column-integrated curves are equivalent to their respective quantities shown in Table 3.

steady state) are not primary contributors to total aerosol forcing.

2.4.3. Particle Asphericity

[42] Irregularly shaped particles have smaller terminal velocities than perfect spheres. The maximum reduction in fall speed for compact irregularly shaped particles is about 25% [*Reist*, 1993]. Reducing terminal fall speed in the model by 25% results in a 5% higher TOAF in the Caribbean compared to base case calculations due to the prolonged lifetimes of the particles.

2.4.4. Subsidence

[43] A large semipermanent region of high pressure exists over the North Atlantic Ocean in the summer. *Carlson and Prospero* [1972] observed that the SAL subsides by 50–100 mb during trans-Atlantic transport, corresponding to a subsidence rate of 1–2 mm s^{-1}. The effect of atmospheric subsidence on dust radiative forcing is examined by including a vertical transport term between model levels in the SAL and underlying layers. Subsidence is assumed to be balanced by an equivalent net downward entrainment transport rate from the free troposphere to the MBL. Subsidence removes particles of all sizes from the SAL to the MBL, where they can be removed by precipitation. Assuming a subsidence rate of 1.5 mm s^{-1} (900 m over 7 days), clear-sky TOAF in the Caribbean is ~20% lower than in the base case.

2.4.5. Coagulation

[44] The modeled evolution of the aerosol plume (Figure 4) shows that concentrations of particles <0.1 μm diameter are reduced by an order of magnitude during the 7 days it is assumed it takes for the plume to cross the Atlantic Ocean. Mass is conserved during coagulation. Relatively small particles removed by coagulation add to the mass of larger particles. However, the mass increase is small (e.g. clay particle mass grows by a maximum of 3% at 0.2 μm diameter and about 0.3% at supermicron sizes). Consequently, coagulation from Brownian motion and gravitational settling does not lead to significant changes in TOAF during long range transport over the Atlantic Ocean.

2.4.6. Dust Mineralogical Composition

[45] The Saharan desert is not mineralogically uniform. A survey of the Ca/Al ratio (an indicator of calcite content) measured by several authors [*Coude-Gaussen et al.*, 1987; *Gomes et al.*, 1990; *Bergametti et al.*, 1989; *Herrmann et al.*, 1999] suggests that calcite forms a larger fraction of dust aerosol derived from soils of northern than of southern origin. Si/Al ratios also show considerable regional variability. XRF measurements from PELTI (Table 7) suggest mineralogical variability between samples.

[46] Quartz and calcite are nonabsorptive at visible wavelengths whereas clay particles commonly contain light absorbing iron oxides. Here we make a rough estimate of the sensitivity of radiative forcing by dust to mineralogical variability. The base mineralogical composition is shown in Table 2. A high (low) clay loading case represents an increase (decrease) of the clay fraction by a factor of 1.25, and a proportional decrease (increase) of the fraction of calcite and quartz in each size range. Quartz and calcite

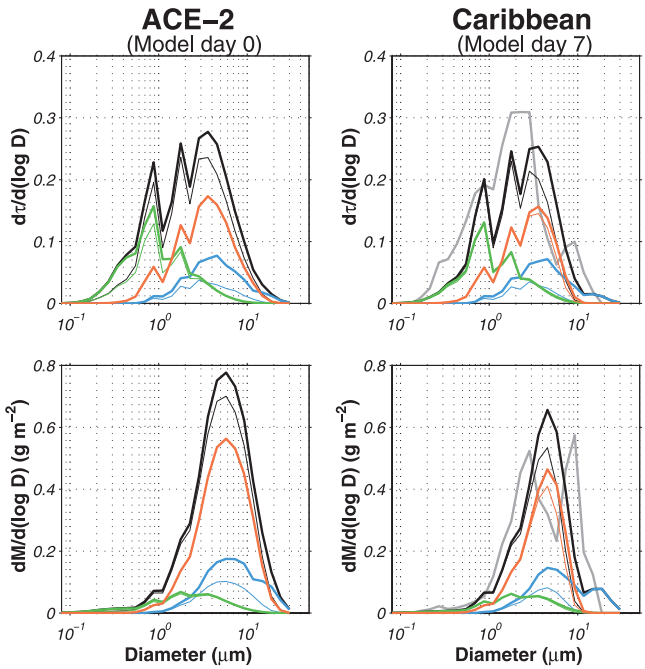

Figure 7. As in Figure 6, except for the ACE-2 17 July initialization case.

have a density similar to that of clays and therefore have similar gravitational settling rates. However, quartz and calcite particles absorb less and scatter more light than clay particles. Therefore, an increase (decrease) in the clay fraction by a factor of 1.25 does not change predicted mass concentrations in the Caribbean. However, it does correspond to a decrease (increase) in the contribution of dust to TOAF by 10% (22%).

3. Comparisons With Measurements From PELTI in the Caribbean

[47] We compare model predictions of microphysical and radiative properties in the Caribbean to measurements obtained during PELTI, and ERBE satellite measurements. The model was initialized using data from ACE-2 on 8 July and 17 July 1997, whereas PELTI took place between 5 July and 23 July 2000. The justification for treating measurements from two projects in July of two different years as an artificial Lagrangian data set, with which the modeled time evolution can be compared, is discussed in section 4.

3.1. Instrumentation

[48] PELTI was based out of St. Croix, United States Virgin Islands. Data from PELTI was collected aboard the NCAR/NSF Research Aviation Facility EC-130Q Hercules aircraft. There were nine research flights during PELTI. They consisted primarily of approximately one hour duration horizontal flight legs over the Caribbean. This flight technique permits measurements of sparsely distributed large particles and of the chemical compositions of low-mass submicron aerosol. Four of these flights, on 9, 15, 19, and 21 July 2000, included flight legs within a dusty SAL in the lower free-troposphere. In addition, on 21 July, the EC-130Q aircraft profiled the SAL to 6 km altitude.

3.1.1. Size Distributions

[49] Particles with sizes between 0.005 and 20 μm diameter were measured aboard the EC-130Q using a radially classified aerosol detector (RCAD) (which samples air drawn into the interior of the aircraft) [*Russell et al.*, 1996], a Particle Measurement Systems (PMS) PCASP-100X (located on the right wing), and a PMS FSSP-300 (located on the left wing). The FSSP-300 obtains measurements of aerosol at ambient relative humidity, whereas the RCAD and PCASP provide measurements of dry aerosol spectra.

[50] The principal errors in PMS probe concentration and size are partially accounted for using an algorithm developed by D. Baumgardner (personal communication). The estimated remaining error is 20% in concentration, 17% in size, and 54% in mass [cf. *Baumgardner et al.*, 1992]. In an aerosol mixture, with differing refractive indices, a volume-weighted average size bin is used to represent the sizing for all species combined.

3.1.2. Composition

[51] The chemical composition of the submicron component of the aerosol size distribution was obtained using a submicron three-stage aerosol virtual impactor located within the EC-130Q research aircraft. The virtual impactor concentrates aerosol between sizes of 0.1 and 1.7 μm with a peak concentration factor of 27 at 0.55 μm and tailing to 50% of peak concentration at 0.3 and 1.1 μm diameter. For mass size distributions measured in the SAL during PELTI, the mean mass concentration factor is 11, dropping to 50% of that value at 0.4 and 1.5 μm diameter. Aerosol particles that pass through the impactor are collected on a Teflon filter. Concentrations of elements with atomic numbers higher than 11 were obtained using X-ray fluorescence (XRF) analysis. Concentrations of organic carbon (OC), sulfate, ammonium and silicate were obtained using Fourier Transform Infrared Spectroscopy (FTIR), with uncertainties of ~10% for the chemical analysis, and ~15% for inlet uncertainties [*Maria et al.*, 2002].

[52] Total aerosol composition was inferred from bulk ion chromatographic analysis of ions on Teflon filters. Filtered particles were drawn into the aircraft using a shrouded solid-diffuser/curved-tube inlet. Estimated concentration errors due to the chemical analysis are 5% for CSN species and 30% for sea-salt, and concentration errors from inlet uncertainties are ~20%. The measurement techniques are described in detail by B. J. Huebert et al. (Measuring the passing efficiency of an airborne low turbulence aerosol inlet, submitted to *Journal of Aerosol Science*, 2002).

3.1.3. Meteorological Parameters

[53] The NCAR EC-130Q research aircraft was equipped with a Rosemount platinum resistance thermometer, an NCAR model crossflow Lyman-Alpha hygrometer, and a Rosemount digital pressure sensor. Horizontal winds were calculated using an inertial navigation system and a gust probe sensor.

3.2. Measurements

3.2.1. Vertical Profile

[54] A vertical profile of the SAL measured during PELTI at approximately 13°N, 60°W on 21 July 2000 shows dust well-mixed between the top of the boundary layer, located at 1.5 km, and a second inversion located at 5 km altitude (Figure 8). The relative humidity was greater than 80% through most of the boundary layer, whereas the dust-laden free troposphere had an average relative humidity of 44 ± 8%. Wind speed and direction were approximately constant through the depth of the MBL and SAL (supporting the column model assumption in this study).

[55] Winds in the SAL were 11.3 ± 0.5 m s^{-1} from the east. Potential temperature increased from 40° to 44° from the bottom to the top of the SAL. Therefore, the SAL was extremely stable (supporting the model assumption of no vertical diffusion). The value of the Richardson number in the dust layer, derived from measured vertical wind and potential temperature profiles, was ~1000.

[56] Values of potential temperature measured in the SAL are consistent with earlier measurements of the Caribbean SAL in July [*Carlson and Prospero*, 1972]. Compared to the profiles for the east side of the tropical North Atlantic Ocean shown in Figure 8, the SAL in the Caribbean is more stable, ~2°C cooler and has a higher relative humidity.

[57] Isobaric back trajectory calculations (Figure 1) indicate that MBL air measured during PELTI followed the trade winds from Western Europe and SAL air could be traced back to West Africa. For the profile sampled on 21 July 2000, the movement of the Saharan dust plume across the Atlantic Ocean could be tracked using TOMS aerosol index (AI) product. AI is a qualitative measure of aerosol absorption. The aerosol plume measured on 21 July 2000 had an AI value of ~2.0. Inspection of successive maps of

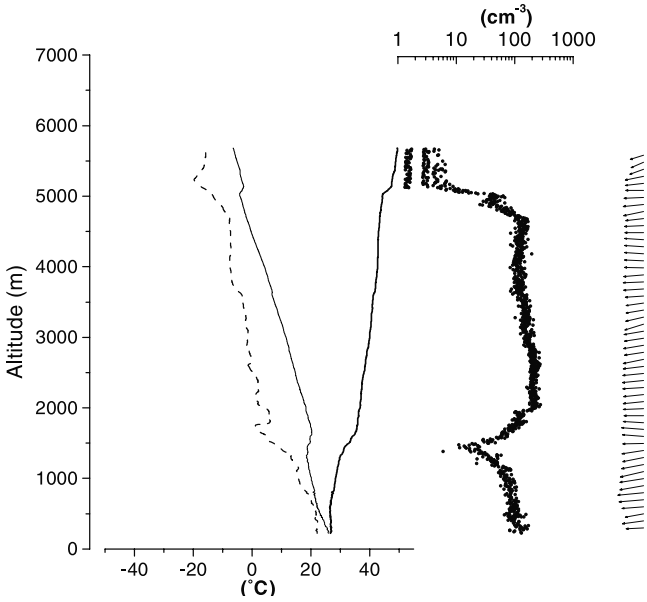

Figure 8. As for Figure 2, except airborne measurements obtained on 21 July 2000 during PELTI.

the AI distribution prior to 21 July suggest the plume had its origins in a dust storm within the Gao province of eastern Mali (17°N, 0°W) on 14 July 2000, where the value of AI was ~3.5.

3.2.2. Particle Size Distributions

[58] Measurements of dust were obtained during horizontal flight legs approximately one hour long within a hazy free troposphere. The samples obtained were from 9 July at 2440 m altitude, 15 July at 2090 m altitude, 19 July at 2920 m altitude, and 21 July at altitudes of 2280, 2770 and 3922 m. Visually, the hazy layers sometimes appeared to be stratified and gently sloping. Since the plane flew at constant altitude, there were times when the plane flew above or below a layer. These time periods had low concentrations of supermicron aerosol and were not included in the mean size distributions for all legs shown in Figure 4. The variability between the mean concentrations measured in each flight leg was ~30%. Maximum concentrations of aerosol were at 0.05 μm on 15 July and 19 July, and 0.02 μm on 21 July. The submicron portion of the size distribution had a slope of ~1.5, whereas the supermicron portion had a slope of ~2.7. The measured mass distribution was bimodal, with maxima at ~2.5 and ~8 μm.

[59] To the extent that ACE-2 and PELTI measurements were representative of aerosols at their respective locations, the model predicted a reduction in concentrations of particles <0.04 μm that was not observed in measurements. A possible mechanism, not included in the model, that might compensate for loss of particles in this size range is nucleation of new aerosol, although this would be surprising given the large preexisting aerosol surface area.

[60] Concentrations of SAL aerosol with diameters between 0.1 and 1 μm were as much as an order of magnitude higher in PELTI than model predictions. It is unlikely this difference is due to instrumentation errors during PELTI. Similar instruments and sizing assumptions were used to initialize the model (based on data from ACE-2) and obtain size distributions during PELTI. Further, instrument sizing uncertainties are relatively small (<0.1 μm). Also, available SO_2 concentrations measured off the West African coast, used to initialize the model, were insufficient to account more than a 1% increase in particle diameter, even if all available SO_2 had condensed and neutralized to form ammonium sulfate (rather than reacted with larger calcite particles). Finally, as discussed in section 2.4.5, coagulation does not significantly change particle mass during transport in the SAL. The observed difference may be indicative of ambient variability (note the agreement is better for the 17 July initialization than the 8 July initialization), or possibly an important process is not accounted for in the model.

[61] The third area of substantial disagreement between model predictions and measurements is for very large particles. First, the measured mass distribution is bimodal, whereas the modeled mass distribution has a single mode at ~4 μm. The bimodality may be an artifact of measuring low particle concentrations, and the compounded uncertainties from inferring mass from sizing measurements. Second, concentrations of particles larger than 10 μm were underpredicted by the model. In fact, particle concentrations were in excellent agreement with measurements of dust size distributions in ACE-2 on the east side of the Atlantic Ocean. This suggests that the removal rate for giant dust aerosol is much smaller than predicted assuming gravitational dry deposition for spheres, or that the source concentrations of large particles for the PELTI event in 2000 were significantly higher than those measured in ACE-2 in 1997.

[62] In the MBL (Figure 5), there is general agreement between measured and predicted size distributions up to ~3 μm diameter (at ambient RH). Most notably, a submicron aerosol mode observed during ACE-2, associated with CSN aerosol, is absent in the PELTI measurements and model predictions. Between 3 and 10 μm diameter agreement between predictions and measurements is poor. This may be because ACE-2 measurements of MBL aerosol in this size range (on which the predicted values are based) relied on a linear extrapolation from PCASP-100X data, which extends only to 3 μm [*Collins et al.*, 2000].

3.3. Aerosol Composition

[63] CSN and sea-salt aerosol concentrations are inferred from bulk filter samples of aerosol composition obtained during 6 flight legs, between 2 and 4 km in a dusty SAL, on four days during PELTI (Table 5). Concentrations of inorganic CSN aerosol are estimated from total concentrations of nitrate, sulfate, and non-sea-salt sulfate. Sea-salt aerosol concentrations are estimated from total sodium, chlorine, and sea-salt sulfate concentrations. Total aerosol concentration is estimated from FSSP-300 measurements averaged over the duration of the filter samples. The difference between total concentrations and the sum of inorganic CSN aerosol and sea-salt is most probably accounted for by dust and organic aerosols, which were not measured. However, measurements from ACE-2 [*Collins et al.*, 2000] suggest carbonaceous aerosol is roughly half of total CSN aerosol concentrations in the free-troposphere (the remainder being sulfate and ammonium compounds). Therefore, PELTI bulk composition data suggest CSN aerosol consisted between 10% and 20% of total aerosol mass, which is consistent with model predictions at 2.75 km altitude in the

Table 5. Average and Standard Deviation of Ambient Chemical Concentrations in the Saharan Air Layer During PELTI, Derived From Bulk Filter Sample Measurements Obtained During Six ~1 h Horizontal Flight Legs Between 2 and 4 km Altitude (Huebert et al., submitted manuscript, 2002)[a]

NH_4^+, μg m^{-3}	NO_3^-, μg m^{-3}	nss-SO_4^{2-}, μg m^{-3}	Total Inorganic Pollution, μg m^{-3}	Sea-Salt, μg m^{-3}	Total Aerosol Mass, μg m^{-3}
0.4 ± 0.2	1.5 ± 0.3	2.2 ± 0.6	4.0 ± 1.0	1.3 ± 0.6	53 ± 12

[a]Total aerosol concentrations were inferred from average FSSP-300 size distribution measurements from the same period as the filter samples.

Caribbean (Figure 3); for the 8 July and 17 July model initializations, 16% and 17% of total aerosol mass, respectively, was due to CSN aerosols. Sea-salt concentrations were overestimated by the model. Measured values were ~2% of total mass, compared to ~15% in the model.

[64] During PELTI, the submicron portion of total aerosol was collected at the same time as bulk filter samples. The chemical composition of the collected mass was analyzed using FTIR and XRF analysis.

[65] SiO_2 is the principal oxide in minerals, and accounts for ~60% of dust aerosol mass [*Game*, 1962]. Its concentration in submicron aerosol was inferred from FTIR silicate bond measurements. Although it appears that dust must dominate total aerosol (Table 5), composition resolved submicron concentrations shown in Table 6 indicate that, in general, CSN aerosol (such as organic carbon, sulfate and ammonium) dominate dust in the submicron aerosol fraction by approximately a factor of two. For comparison, the modeled ratios of submicron CSN aerosol to dust (which includes all oxides plus bound water) were 3.1 and 2.2 for the 8 July and 17 July initializations, respectively.

[66] Aerosol origin can sometimes be determined from its elemental *enrichment factor* (EF), defined here with respect crustal elemental concentrations published by *Mason* [1966]:

$$\mathrm{EF}_X = \frac{(X/\mathrm{Al})_{measured}}{(X/\mathrm{Al})_{reference}} \tag{3}$$

Al is used as a reference element due to its relative absence in anthropogenic sources and its predominance in the Earth's crust. Average enrichment factors for the submicron aerosol filter samples collected during PELTI are shown in Table 7. Si, Fe, Ca, K, and Ti have enrichment factors near 1, suggesting, as expected, a crustal origin for these elements. Values of EF for S and Cl, by contrast, are ~2 orders of magnitude higher and more variable between samples. In fact, in the samples obtained on 9 July and 19 July, after Si, S was the second largest measured elemental component of the aerosol by mass. In addition, on 21 July, Cl and S were highly enriched at altitudes as high as 3.9 km. The S may have been partially in the form of gypsum ($CaSO_4 \cdot 2H_2O$), formed during heterogeneous reactions of calcite with SO_2 in the atmosphere. However, if this were the case, the molar ratio of S to Ca would be approximately less than or equal to unity, provided most sulfur was in the form of SO_4^{2-} (which, on average, appeared true based on comparisons between XRF sulfur and FTIR SO_4^{2-} concentrations derived from SAL aerosol samples from PELTI). In the submicron component of the aerosol measured during PELTI, the molar ratio of S to Ca was 3.5 ± 0.6, 3.6 ± 0.6, and 1.5 ± 0.3 for three of the six samples and approximately unity in the remainder. The high value of EF for dust, combined with the high S to Ca ratios, suggests submicron SO_4^{2-} measured during PELTI existed in the form of nonmineral sulfate aerosol.

[67] The chemical measurements from PELTI suggest dust particles dominate bulk composition in the SAL, however the submicron component is dominated by CSN aerosol such as organic and sulfate species. This conclusion is in qualitative agreement with the mass distributions shown in Figures 6 and 7, and it is consistent with free-troposphere measurements during dust events in ACE-2 that suggest nonmineral CSN aerosol consists roughly half of total submicron aerosol mass [*Putaud et al.*, 2000]. These aerosols are highly enriched in S relative to crustal soils, even at high altitudes. Combined with the likely absence of vertical mixing of SO_4^{2-} from the MBL into the SAL, these data suggest the origin of CSN aerosols is neither crustal nor the Atlantic Ocean. In section 4 we argue that the CSN aerosol are anthropogenic and originate from Europe. High values of EF for Cl in the SAL possibly indicate a Mediterranean source.

3.3.1. Mass Profile

[68] Mass profiles obtained in the Caribbean during PELTI are shown in Figure 3 alongside predictions. The profiles are a composite of size distribution profiles obtained during PELTI in the SAL on 21 July 2000, and boundary layer profiles obtained on 9, 15, 19, and 21 July 2000. Dust aerosol forms a 4 km thick layer between 1.2 and 5.2 km, which is nearly identical to the location in the 8 July model predictions. The maximum total mass concentration within the SAL is 75 μg m^{-3}, which is within 5% of predictions for the 8 July case, but is slightly more than half of peak concentrations predicted for the 17 July case.

3.3.2. Column-Integrated Mass and Optical Depth Distributions

[69] Compared with model predictions (Figures 6 and 7), measured column-integrated mass and optical depth distributions are in approximate agreement. The measured peak for mass and optical depth are located at 3 μm and 2.5 μm diameter, respectively, compared to 4.5 μm and 3.5 μm, respectively for the model. The supermicron fraction of the optical depth distribution dominates optical extinction. This is consistent with

Table 6. Average and Standard Deviation of Ambient Concentrations of Organic Carbon (OC), Ammonium, Total Sulfate, and Equivalent SiO_2[a], Inferred From FTIR Analyses of Filter Samples of Submicron Aerosol Obtained During ~1 h Horizontal Flight Legs in the Saharan Air Layer During PELTI [*Maria et al.*, 2002]

OC , μg m^{-3}	NH_4^+, μg m^{-3}	SO_4^{2-}, μg m^{-3}	Equivalent SiO_2, μg m^{-3}
1.1 ± 0.7	0.2 ± 0.1	0.8 ± 0.4	0.6 ± 0.2

[a]Calculated from measured Si_2O_5, SiO_2, and SiO_4^{4-} absorbance.

Table 7. Average and Standard Deviation of Elemental Enrichment Factors (EF), With Respect to Reference Crustal Element Al, Derived From XRF Analyses of Filter Samples of Submicron Aerosol Obtained During ~1 h Horizontal Flight Legs in the Saharan Air Layer During PELTI [*Maria et al.*, 2002][a]

Si	Fe	Ca	K	Ti	S	Cl
0.62 ± 0.09	1.08 ± 0.16	0.79 ± 0.24	0.59 ± 0.12	1.36 ± 0.4	168 ± 180	58 ± 47

[a]The sample on 9 July 2000 was excluded because Al concentrations had a relative error exceeding 30%.

visual observations during flight in the SAL. The haze layer was milky white, independent of direction relative to the Sun (i.e. spectral extinction was optically flat). For supermicron aerosol, at visible wavelengths, the extinction efficiency is approximately independent of wavelength. In general measured mass and optical depth were larger at submicron sizes and smaller at supermicron sizes compared to model predictions.

3.3.3. Direct Clear-Sky Shortwave Radiative Forcing

[70] We predicted that TOAF decreases by between 10% and 20% for the cases studied here. This value is surprisingly small considering the 7 day simulation time of the model. No direct measurements of TOAF are available from PELTI. However, we can make some qualitative comparisons between model results and mean July satellite measurements from the 1985–1988 Earth Radiation Budget Experiment (ERBE) [*Harrison et al.*, 1990]. Figure 9 shows shortwave radiative forcing by aerosols over the North Atlantic Ocean. Values of TOAF are inferred by subtracting measured ERBE clear-sky shortwave outgoing flux data from gases-only fluxes calculated with the shortwave radiative transfer model (section 2.1.2). The primary errors associated with values of TOAF inferred from ERBE over oceans are associated with the cloud-removal algorithm. ERBE has a large "footprint" (2.5° × 2.5°) and subgrid scale trade wind cumulus are common in the region of interest. *Loeb and Kato* [2002] estimated the magnitude of this bias is ≈−4 W m^{-2}.

[71] It is not possible to make a direct comparison between aerosol forcing within the broad plume of high aerosol forcing shown in Figure 9, and the model results shown in Tables 3 and 4. The model results track evolution of a specific dust event, whereas Figure 9 shows a spatial representation of the temporally averaged aerosol forcing. Further, Figure 9 gives no information about the relative contributions of different aerosol types to TOAF. However, the temporal gradient in total TOAF, inferred from results shown in Tables 3 and 4, is analogous to the temporally averaged spatial gradient shown in Figure 9 provided localized sources of aerosol are uniform along the length of the plume. Sea-salt aerosol are the principal such source. Over the oceans, they are produced by high wind speeds over the oceans. Along 17°N, over the tropical North Atlantic Ocean, the Special Sensor Microwave Imager (SSMI) shows the average wind speeds are 7.5 ± 0.5 m s^{-1}.

[72] If the estimated cloud contamination bias of −4 W m^{-2} is removed from Figure 9, the magnitude of the forcing is approximately −11 W m^{-2} near the Canary

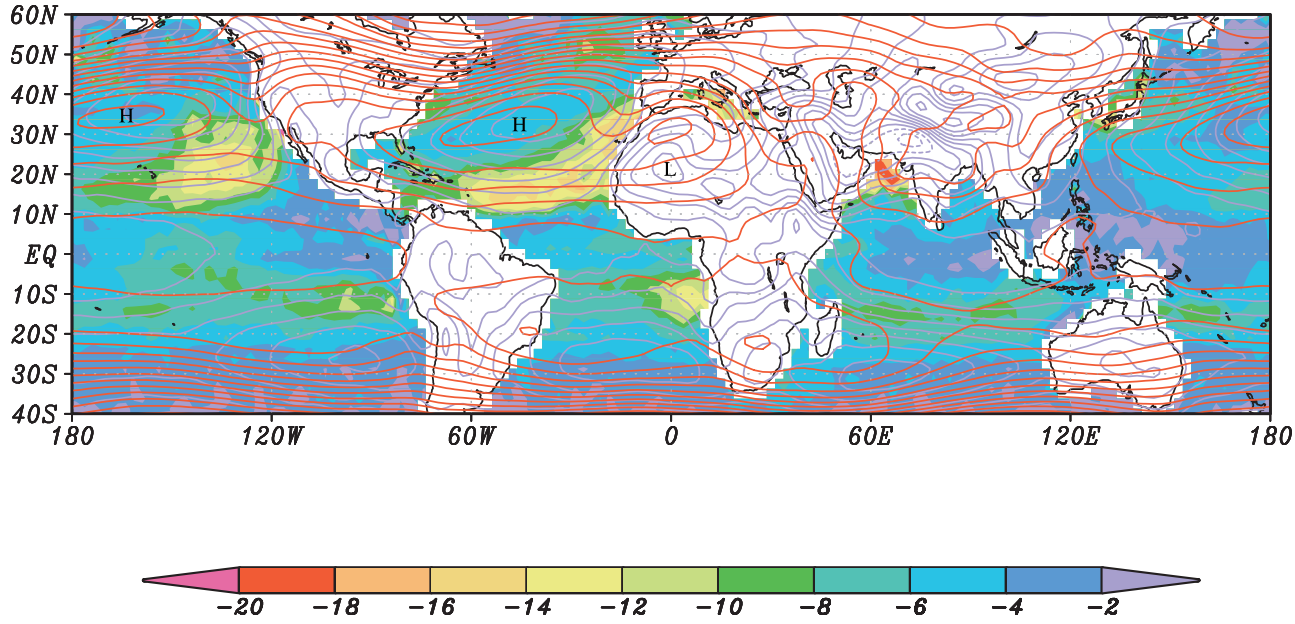

Figure 9. Mean July clear-sky aerosol direct shortwave radiative forcing in W m^{-2} over the oceans (shaded contours), inferred from the 1985–1988 ERBE clear-sky data set. Lines are 16 mb contours of the mean July geopotential height field at 1000 mb (purple lines) and 700 mb (red lines) from the 1958–1997 NCEP reanalysis data set.

Islands at 15°W. This value is consistent with estimates based on the 8 July and 17 July case studies shown in Tables 3 and 4. Southwest of this region there extends a broad region of high aerosol forcing that shifts westward over the North Atlantic at a latitude of approximately 17°N. Sea-salt aerosol are likely responsible for a significant fraction of this forcing. *Loeb and Kato* [2002] found that in the trade winds over the North Pacific, far from dust and pollution sources, a wind speed of 7.5 ± 0.5 m s^{-1} corresponds to a direct shortwave radiative effect of -3.5 ± 2 W m^{-2}, which is within 15% of predicted values. Peak values of aerosol forcing in the center of the plume are roughly undiminished as far as 50°W. The magnitude of aerosol forcing drops off significantly only when the plume reaches the Caribbean Sea, where the SAL has cooled somewhat and convective activity may be sufficient for cumulus clouds to penetrate into the SAL.

[73] Although model results track specific events, whereas Figure 9 represents a monthly mean over four years, aerosol forcing from ERBE data and the model agree to within 25%. Further the estimated fraction of direct radiative forcing from sea-salt is consistent with model estimates. Finally, both the spatial gradient shown in ERBE data, and model predictions of the evolution of a plume, suggest TOA forcing across the tropical North Atlantic Ocean decreases by less than ~20% between Africa and the Caribbean.

4. Discussion

[74] A prominent feature of global aerosol optical depth in the summer is a broad plume, associated with Saharan dust, that extends westward from the African continent to the Caribbean. This study addresses the microphysical and radiative evolution of aerosol plumes over the tropical North Atlantic Ocean in July. An explicit 1-D chemical and microphysical model was used, linked to a shortwave radiative transfer model. The model was initialized using measurements in the boundary layer and lower free troposphere near the Canary Islands off the West African coast, obtained on two days in July 1997 during ACE-2 when there was a dusty SAL. Predicted microphysical and radiative properties were compared with airborne measurements from the Caribbean collected on four days in July 2000 during PELTI, and with mean July clear-sky ERBE satellite data from 1985 to 1988.

[75] Since simultaneous airborne field campaigns have not been conducted in both locations, a pure Lagrangian study was not possible, which constrains conclusions that might be drawn from comparing the two data sets. Further, only two dust events were measured by aircraft during ACE-2, and only four during PELTI. However, evidence suggesting measurements from both field campaigns are representative of similar events include a) TOMS imagery and back-trajectory calculations suggest SAL dust aerosol measured during PELTI and ACE-2 originated from Mali, Saharan Africa (sections 2.2 and 3.2.1), b) MBL back-trajectories from PELTI traced back to near the ACE-2 region (Figure 1), and c) measured potential temperature profiles during dust events were similar to equivalent measurements of the phenomenon recorded by *Carlson and Prospero* [1972] (sections 2.2 and 3.2.1).

[76] We showed a broad consistency between model predictions and measurements. The plume has two layers. The bottom layer is dominated by sea-salt aerosol in the MBL and the top layer is approximately 3 km deep in the lower free-troposphere and is dominated by mineral dust. The mode mass diameter of the dust shifts from ~6 μm to ~4 μm following long-range transport across the Atlantic Ocean. CSN aerosol are the major component of SAL aerosol mass at submicron sizes. Model results and ERBE data suggest clear-sky direct radiative forcing by aerosols decreases by less than ~20% while crossing the Atlantic Ocean.

[77] Nonetheless, there were significant discrepancies between predicted and measured size distributions in the Caribbean (Figures 4 and 5). In the MBL, the model overpredicted aerosol concentrations in the 4 to 10 μm diameter size range compared to measurements, possibly due to the extrapolation used in that size range by *Collins et al.* [2000]. The effect of this potential error on our conclusion that MBL sea-salt contribute significantly to total TOAF is small, however, since Collins et al. found MBL aerosol in this size range make a minor contribution to total MBL extinction. In the model, SAL aerosol in the 0.1 to 1.0 μm size range, which contribute to ~20% of column τ in the Caribbean (Figures 6 and 7), had measured concentrations as much as one order of magnitude higher, or sizes twice as large as predictions. As discussed in section 3.2.2, it is difficult to attribute this discrepancy to instrument error, particle coagulation, or heterogeneous chemical reactions during long-range transport. However, measurements obtained during PELTI and ACE-2 suggest submicron aerosols in the SAL are primarily CSN, and that they exhibit much greater variability in their concentrations than do mineral aerosols (section 3.3). In this case, it is possible that measurements in the SAL during ACE-2, and model predictions in the Caribbean, represent opposing ends of the climatological range of submicron CSN aerosol concentrations and radiative forcing.

[78] The presence of significant quantities of CSN aerosol within the SAL during dust events has been noted previously in the Caribbean [*Talbot et al.*, 1986] and off the coast of West Africa [*McGovern et al.*, 1999; *Maring et al.*, 2000; *Putaud et al.*, 2000]. Long term surface measurements in Barbados [*Savoie et al.*, 1989] show that sulfate mass concentrations correlate linearly with dust mass and that 30% of this mass is in the fine fraction (<1 μm diameter). *Maring et al.* [2000] found that nonmineral aerosol contribute to 34% of total scattering in the SAL in the late summer. Model calculations presented here suggest CSN aerosol contribute to about one third of total optical depth over the tropical North Atlantic Ocean during dust events, and also to about 20% of TOAF. Measurements from PELTI suggest these aerosol are not Saharan in origin and that they are mixed externally with the dust (section 3.3).

[79] What is the origin of these CSN aerosols if not the Sahara? The potential temperature is ~20 K higher in the SAL than in the MBL, so it is unlikely surface convection lofted biogenic marine aerosol from the MBL into the free-troposphere over the North Atlantic Ocean. Rather, we suggest the CSN aerosols were man-made emissions of European origin that were carried with the dust as the air crossed the Sahara. Overlying the TOAF field shown in

Figure 9, are the National Center for Environmental Prediction (NCEP) reanalysis mean July 1000 mb and 700 mb geopotential height fields. The 1000 mb pressure field indicates air crosses the Mediterranean Sea from Central or Eastern Europe to the central Saharan desert. According to the meteorological mechanism discussed in section 1, the air is heated over the Sahara, lofted into the lower free-troposphere, and transported in the SAL by the easterly jet at 17°N to the Caribbean (see the 700 mb pressure field in Figure 9). Thereby, the SAL may be a conduit not only for dust, but also for long-range transport of pollution from Europe to the Caribbean.

[80] Surface flow (1000 mb) over the tropical North Atlantic Ocean is dominated by the remarkably steady easterly trade winds, which, like the SAL, transport air westward at ~17°N (Figure 9). When northerly precursors to the tradewinds carry air from Western Europe (as they did for the 8 July case from ACE-2) the MBL may also contain pollution. However, these aerosol are likely removed by precipitation over the ocean within a few days. On the other hand, trade winds provide a steady source for sea-salt. Note that in Figure 9, large values of aerosol forcing are in broad bands associated with trade wind flow over the remote northern and southern oceans. Therefore, the satellite imagery supports the model conclusions that high values of aerosol forcing over the tropical North Atlantic Ocean are due in part to sea-salt.

[81] In summary, our interpretation of NCEP climatology, back-trajectories from the Caribbean during PELTI, field measurements and model results is that air masses in the MBL and SAL during July have different origins but overlay one another over much of the tropical North Atlantic Ocean. The net result is that the radiative impact of aerosols can be seen as arising from two layers. Pollution from Western European and sea-salt dominates radiative properties in the MBL; European pollution and Saharan dust dominate in the SAL. Even for the specific plumes examined here, which are essentially "dust" events, sea-salt and pollution components yield a significant contribution to τ and TOAF. Examination of monthly and seasonal means, rather than individual cases, could further amplify this effect since sea-salt represents a continuous background forcing. Further, unlike sea-salt, mineral aerosol have no source over the Atlantic Ocean, and unlike pollution aerosols, which dominate at small sizes, mineral aerosol are removed from the SAL by gravitational settling. Therefore the relative contribution of mineral aerosol to total aerosol forcing over the Atlantic Ocean decreases with time.

[82] The degree to which dust contributes to aerosol forcing over the tropical North Atlantic is particularly sensitive to atmospheric subsidence, which, due to a region of semipermanent high pressure over the North Atlantic ocean in the summer, is on the order of 100 m day^{-1}. The reduction of TOAF by dust due to subsidence during transport is comparable to that due to gravitational settling. Naturally, removal is slowed if the SAL starts from a higher altitude. (In contrast to summer dust events, springtime Harmattan dust transport is near the surface, and therefore it may be expected to have a shorter lifetime over the Atlantic Ocean). Dust forcing is also sensitive to assumed mineralogy, which appears variable based on elemental analysis data from PELTI, model calculations show a 25% decrease in the assumed fractional contribution of clays to total dust corresponds to a 22% increase in the contribution of dust to TOAF.

[83] Further studies are needed to address the uncertainties associated with the contribution of CSN aerosol to the evolution of radiative forcing within the SAL. Ideally these measurements should focus on the size-resolved composition of SAL aerosol on both sides of the Atlantic associated within an individual dust event. In particular, further measurements are required to ascertain the relative contributions of submicron chemically generated and mineral aerosol with high specific extinction. Finally, models must resolve the vertical particle distribution and subsidence of the SAL to accurately describe its radiative evolution.

[84] **Acknowledgments.** This research was supported by the Princeton Environmental Institute, and NSF grant 9732949 and NASA grant NAG5-8676 to Princeton University. We are grateful to Don Collins, Hal Maring and Marian deReus for providing data used in this study, and to Krista Laursen for her coordination of PELTI.

References

Baumgardner, D., J. E. Dye, B. W. Gandrud, and R. G. Knollenberg, Interpretation of measurements made by the forward scattering spectrometer probe (FSSP-300) during the Airborne Arctic Stratospheric Expedition, *J. Geophys. Res.*, *97*, 8035–8046, 1992.

Bergametti, G., L. Gomes, G. Coude-Gaussen, P. Rognon, and M. N. le Coustumer, African dust observed over Canary Islands: Source-regions identification and transport pattern for some summer situations, *J. Geophys. Res.*, *94*, 14,855–14,864, 1989.

Bohren, C. F., Applicability of effective-medium theories to problems of scattering and absorption by nonhomogeneous atmospheric particles, *J. Atmos. Sci.*, *43*, 468–474, 1986.

Böke, H., H. Göktürk, E. N. Caner-Saltik, and S. Demirci, Effect of airborne particle on SO_2–calcite reaction, *Appl. Surf. Sci.*, *140*, 70–82, 1999.

Cakmur, R. V., R. L. Miller, and I. Tegen, A comparison of seasonal and interannual variability of soil dust aerosols over the Atlantic Ocean as inferred by the TOMS AI and AVHRR AOT retrievals, *J. Geophys. Res.*, *106*, 18,287–18,303, 2001.

Carlson, T. N., and R. S. Caverly, Radiative characteristics of Saharan dust at solar wavelengths, *J. Geophys. Res.*, *82*, 3141–3152, 1977.

Carlson, T. N., and J. M. Prospero, The large scale movement of Saharan air outbreaks over the northern equatorial Atlantic, *J. Appl. Meteorol.*, *11*, 283–297, 1972.

Chiapello, I., G. Bergametti, B. Chatenet, F. Dulac, I. Jankowiak, C. Liousse, and E. S. Soares, Contribution of the different aerosol species to the aerosol mass load and optical depth over the northeastern tropical Atlantic, *J. Geophys. Res.*, *104*, 4025–4035, 1999.

Claquin, T., M. Schulz, Y. Balkanski, and O. Boucher, Uncertainties in assessing radiative forcing by mineral dust, *Tellus*, *50B*, 491–505, 1998.

Collins, D. R., et al., In situ aerosol-size distribution and clear-column radiative closure during ACE-2, *Tellus*, *52B*, 498–525, 2000.

Coude-Gaussen, G., P. Rognon, G. Bergametti, L. Gomes, B. Strauss, J. M. Gros, and M. N. Le Coustumer, Saharan dust of Fuerteventura Island (Canaries): Chemical and mineralogical characteristics, air mass trajectories, and probable sources, *J. Geophys. Res.*, *92*, 9753–9771, 1987.

de Reus, M., F. Dentener, A. Thomas, S. Bormann, J. Ström, and J. Lelieveld, Airborne observations of dust aerosol over the North Atlantic Ocean during ACE-2: Indications for heterogenous ozone destruction, *J. Geophys. Res.*, *105*, 15,263–15,275, 2000.

Dentener, F. J., G. R. Carmichael, Y. Zhang, J. Lelieveld, and P. J. Crutzen, Role of mineral aerosol as a reactive surface in the global troposphere, *J. Geophys. Res.*, *101*, 22,869–22,889, 1996.

Dubief, J., Review of the North African climate with particular emphasis on the production of eolian dust in the Sahel zone and in the Sahara, in *Saharan Dust*, edited by C. Morales, 297 pp., John Wiley, New York, 1977.

Formenti, P., M. O. Andreae, and J. Lelieveld, Measurements of aerosol optical depth above 3570 m asl in the North Atlantic free troposphere: Results from ACE-2, *Tellus*, *52B*, 678–693, 2000.

Freidenreich, S. M., and V. Ramaswamy, A new multiple band solar radiative parameterization for GCM's, *J. Geophys. Res.*, *104*, 31,389–31,409, 1999.

Game, P. M., Observations on a dustfall in the Eastern Atlantic, February, 1962, *J. Sediment. Petrol.*, *34*, 355–359, 1962.

Glaccum, R. A., and J. M. Prospero, Saharan aerosols over the tropical North Atlantic—Mineralogy, *Mar. Geol.*, *37*, 295–321, 1980.

Gomes, L., G. Bergametti, G. Coude-Gaussen, and P. Rognon, Submicron desert dust: A sandblasting process, *J. Geophys. Res.*, *95*, 13,297–13,935, 1990.

Gonzales, T. W., and L. E. Murr, An electron microscopy study of particulates present in individual raindrops, *J. Geophys. Res.*, *82*, 3161–3166, 1977.

Harrison, E. F., P. Minnis, B. R. Barkstrom, V. Ramanathan, R. D. Cess, and G. G. Gibson, Seasonal variation of cloud radiative forcing derived from the Earth Radiation Budget Experiment, *J. Geophys. Res.*, *95*, 18,687–18,703, 1990.

Haywood, J. M., V. Ramaswamy, and B. J. Soden, Tropospheric aerosol climate forcing in clear-sky satellite observations over the oceans, *Science*, *283*, 1299–1303, 1999.

Haywood, J. M., P. N. Francis, M. D. Glew, and J. P. Taylor, Optical properties and direct radiative effect of Saharan dust: A case study of two Saharan dust oubreaks using aircraft data, *J. Geophys. Res.*, *106*, 18,417–18,430, 2001.

Herring, J. A., R. J. Ferek, and P. V. Hobbs, Heterogeneous chemistry in the smoke plume from the 1991 Kuwait oil fires, *J. Geophys. Res.*, *101*, 14,451–14,463, 1996.

Herrmann, L., K. Stahr, and R. Jahn, The importance of source region identification and their properties for soil-derived dust: The case of Harmattan dust sources for eastern West Africa, *Contrib. Atmos. Phys.*, *72*, 141–150, 1999.

Ivlev, L. S., and S. I. Popova, Optical constants of substances of atmospheric aerosols, *Izv. Vysov. Fiz.*, *5*, 91–97, 1972.

Johnson, D. W., et al., An overview of the Lagrangian experiments undertaken during the North Atlantic regional Aerosol Characterisation Experiment (ACE-2), *Tellus*, *52B*, 290–320, 2000.

Kahn, R., P. Banerjee, and D. McDonald, Sensitivity of multiangle imaging to natural mixtures of aerosols over the ocean, *J. Geophys. Res.*, *106*, 18,219–18,238, 2001.

Li, X., H. Maring, D. Savoie, K. Voss, and J. M. Prospero, Dominance of mineral dust in aerosol light-scattering in the North Atlantic trade winds, *Nature*, *380*, 416–419, 1996.

Li-Jones, X., H. B. Maring, and J. M. Prospero, Effect of relative humidity on light scattering by mineral dust aerosol as measured in the marine boundary layer over the tropical Atlantic Ocean, *J. Geophys. Res.*, *103*, 31,113–31,121, 1998.

Loeb, N. G., and S. Kato, Top-of-atmosphere direct radiative effect of aerosols over the tropical oceans from the Clouds and the Earth's Radiant Energy System (CERES) satellite instrument, *J. Clim.*, *15*, 1474–1484, 2002.

Maria, S. F., L. M. Russell, B. J. Turpin, and R. J. Porcja, FTIR measurements of functional groups and organic mass in aerosol samples over the Caribbean, *Atmos. Environ.*, in press, 2002.

Maring, H., D. L. Savoie, M. A. Izaguirre, C. McCormick, R. Arimoto, J. M. Prospero, and C. Pilinis, Aerosol physical and optical properties and their relationship to aerosol composition in the free troposphere at Izaña, Tenerife, Canary Islands, during July 1995, *J. Geophys. Res.*, *105*, 14,677–14,700, 2000.

Mason, B., *Principles of Geochemistry*, 3rd ed., 329 pp., John Wiley, New York, 1966.

McGovern, F. M., F. Raes, R. VanDingenen, and H. Maring, Anthropogenic influences on the chemical and physical properties of aerosols in the Atlantic subtropical region during July 1994 and July 1995, *J. Geophys. Res.*, *104*, 14,309–14,319, 1999.

Mishchenko, M. I., L. D. Travis, R. A. Kahn, and R. A. West, Modeling phase functions for dustlike tropospheric aerosols using a shape mixture of randomly oriented polydisperse spheroids, *J. Geophys. Res.*, *102*, 16,831–16,847, 1997.

Patterson, E. M., Optical properties of the crustal aerosol: Relation to chemical and physical characteristics, *J. Geophys. Res.*, *86*, 3236–3246, 1981.

Prospero, J. M. The chemical and physical properties of marine aerosols: An introduction, in *Chemistry of Marine Water and Sediments*, edited by A. Gianguzza et al., pp. 35–82, Springer-Verlag, New York, 2002.

Prospero, J. M., and T. N. Carlson, Vertical and areal distribution of Saharan dust over the western equatorial North Atlantic Ocean, *J. Geophys. Res.*, *77*, 5255–5265, 1972.

Putaud, J.-P., et al., Chemical mass closure and assessment of the origin of the submicron aerosol in the maring boundary layer and the free troposphere at Tenerife during ACE-2, *Tellus*, *52B*, 141–168, 2000.

Querry, M. R., Optical constants of minerals and other materials from the millimeter to the ultraviolet, *Rep. No. CRDEC-CR-88,009*, U.S. Army Armament Munitions Chem. Command, Aberdeen Proving Ground, Md., 1987.

Reed, R. J., J. C. Norquist, and E. E. Recker, The structure and properties of African wave disturbances as observed during phase III of GATE, *Mon. Weather Rev.*, *105*, 317–333, 1977.

Reist, P. C., *Aerosol Science and Technology*, 2nd ed., 375 pp., McGraw-Hill, New York, 1993.

Russell, L. M., and J. H. Seinfeld, Size and composition resolved externally mixed aerosol model, *Aerosol Sci. Technol.*, *28*, 403–416, 1998.

Russell, L. M., S.-H. Zhang, R. C. Flagan, and J. H. Seinfeld, Radially classified aerosol detector for aircraft-based submicron aerosol measurements, *J. Atmos. Oceanic Technol.*, *13*, 598–609, 1996.

Savoie, D. L., J. M. Prospero, and E. S. Saltzman, Non-sea-salt sulfate and nitrate in trade wind aerosols at Barbados: Evidence for long-range transport, *J. Geophys. Res.*, *94*, 5069–5080, 1989.

Schulz, M., Y. J. Balkanski, W. Guelle, and F. Dulac, Role of aerosol size distribution and source location in a three-dimensional simulation of a Saharan dust episode tested against satellite-derived optical thickness, *J. Geophys. Res.*, *103*, 10,579–10,592, 1998.

Segelstein, D. J., The complex refractive index of water, M.S. thesis, 67 pp., Univ. of Mo.-Kansas City, Kansas City, 1981.

Shettle, E. P., and R. W. Fenn, *Tech. Pap. AFGL-TR-79-0214*, Air Force Geophys. Lab., Hanscom Air Force Base, Hanscom, Mass., 1979.

Sokolik, I. N., and O. B. Toon, Incorporation of mineralogical composition into models of the radiative properties of mineral aerosol from UV to IR wavelengths, *J. Geophys. Res.*, *104*, 9423–9444, 1999.

Talbot, R. W., R. C. Harris, E. V. Browell, G. L. Grebory, D. I. Sebacher, and S. M. Beck, Distribution and geochemistry of aerosols in the Tropical North Atlantic troposphere: Relationship to Saharan dust, *J. Geophys. Res.*, *91*, 5173–5182, 1986.

Taylor, J. P., J. M. Edwards, M. D. Glew, P. Hignett, and A. Slingo, Studies with a flexible new radiation code, 2, Comparisons with aircraft shortwave observations, *Q. J. R. Meteorol. Soc.*, *122*, 839–861, 1996.

Tegen, I., and A. Lacis, Modeling of particle size distribution and its influence on the radiative properties of mineral dust aerosol, *J. Geophys. Res.*, *101*, 19,237–19,244, 1996.

Tegen, I., P. Hollrig, M. Chin, I. Fung, D. Jacob, and J. Penner, Contribution of different aerosol species to the global aerosol extinction optical thickness, *J. Geophys. Res.*, *102*, 23,895–23,915, 1997.

Twomey, S., and T. A. Wojciechowski, Observations of the geographic variations of cloud nuclei, *J. Atmos. Sci.*, *26*, 687–688, 1969.

Ullerstam, M., R. Vogt, S. Langer, and E. Ljungströ, A diffuse relectance FTIR study of the mechanism and uptake kinetics of SO_2 on mineral dust, paper presented at the *8th European Symposium on the Physico-Chemical Behaviour of Atmospheric Pollutants*, Torino, Italy, September, 2001.

Warren, D., and J. H. Seinfeld, Simulation of aerosol size distribution evolution in systems with simultaneous nucleations, condensation and coagulation, *Aerosol Sci. Technol.*, *4*, 31–43, 1985.

Welton, E. J., et al., Ground-based lidar measurements of aerosols during ACE-2: Instrument description, results, and comparisons with other ground-based and airborne measurements, *Tellus*, *52B*, 636–651, 2000.

Zemaitis, J. F., (Ed.), *Handbook of Aqueous Electrolyte Thermodynamics*, McGraw-Hill, New York, 1986.

T. J. Garrett, Meteorology Department, University of Utah, 135 S 1460 E, Salt Lake City, UT 84112-0110, USA. (tgarrett@met.utah.edu)

B. J. Huebert, School of Ocean and Earth Science and Technology, University of Hawaii at Manoa, Honolulu, HI, USA.

S. F. Maria, Department of Chemical Engineering, Princeton University, Princeton, NJ, USA.

V. Ramaswamy and L. M. Russell, Atmospheric and Oceanic Sciences Program, Princeton University, Princeton, NJ, USA.